COMBUSTION SCIENCE AND TECHNOLOGY
2022, VOL. 194, NO. 12, 2558–2579
https://doi.org/10.1080/00102202.2021.1890055

Taylor & Francis
Taylor & Francis Group

ARTICLE

Pyrolysis and Combustion Characteristics of Leaf-like Fuel under Convection and Radiation Heating

Peyman Rahimi Borujerdi and Babak Shotorban

Department of Mechanical and Aerospace Engineering, The University of Alabama in Huntsville, Huntsville, Alabama, USA

ABSTRACT

The heating of a fuel element representing a vertically oriented living manzanita leaf was computationally investigated. The computational conditions resembled a previous experimental setup where manzanita leaves were exposed to an upward stream of hot gases supplying the convective heating and a radiant panel providing the radiative heating. The simulations confirmed the experimental observations as to what the impact of the heating mode is on ignition. The convection-only and combined convection and radiation modes resulted in ignition and flaming whereas the radiation-only mode did not. The leaf mass loss versus time, the heating pattern of the leaf, the ignition time, and the flame spread pattern in simulations were in good agreement with the experimental findings. Furthermore, the simulations revealed the impact of the heating mode on thermochemical evolution of the leaves, formation of boundary layers on the leaf faces, ignition, and formation and propagation of the flame. An analysis based on the postprocessing of the numerical data showed that except for the first second, the fuel may be considered thermally thin. Ignition occurred near the lower corners of the leaf, which were exposed to the highest heat fluxes compared to the rest of the leaf. In the combined heating mode, the fuel pyrolyzed faster and ignition occurred earlier because the overall heat flux was larger. The computed heat release rates per unit volume showed that the flame is formed in the lower part of the leaf, and then moves and propagates upward. The computations revealed that the overall heat release by combustion of pyrolysis gas was not sensitive to the mode of heating.

ARTICLE HISTORY
Received 8 August 2016
Revised 17 November 2020
Accepted 18 November 2020

KEYWORDS
Pyrolysis; combustion; wildfires; live fuels; convection; radiation; flame propogation

Introduction

Wildfires commonly involve burning of fuel elements such as leaves, twigs and branches. Leaves, in particular, play a critical role in the torching of elevated fuel such as trees and shrubs and consequently in the spread of fires in woodlands and shrublands, e.g., chaparral (Li, Mahalingam, Weise 2017; Prince, Shen, Fletcher 2017; Weise et al. 2016, 2005). This has motivated several experimental and computational studies focused on the burning behavior of individual shrub leaves such as manzanita (arctostaphylos glandulosa). These studies dealt with how living and dead leaves respond to heating while examining the influence of the heating

CONTACT Babak Shotorban babak.shotorban@uah.edu Department of Mechanical and Aerospace Engineering, The University of Alabama in Huntsville, Huntsville, Alabama 35899, USA.

This article has been republished with a minor change. This change does not impact the academic content of the article.

modes and the fuel moisture content (FMC) on moisture evaporation, pyrolysis, ignition and flaming behavior of the leaves.

Experimental investigations of burning behavior of shrub leaves were carried out, using flat-flame burners (FFBs) as the source of convective heating and/or radiative panels (Engstrom et al. 2004; Gallacher 2016; Gallacher et al. 2014; Pickett et al. 2010; Prince 2014; Prince and Fletcher 2014; Yashwanth et al. 2015). The heating mode of FFBs was determined to be almost entirely convective with minimal thermal radiation. Engstrom et al. (2004) conducted burning experiments on four types of plant species representative of California chaparral including manzanita, oak, ceanothus and chamise. Engstrom et al. (2004) observed that for the vertically oriented leaf samples, ignition first occurred at the bottom edge whereas for the horizontally oriented ones, it took place in the vicinity of the sample tip. Pickett et al. (2010) investigated the burning of individual foliage samples from the western and southern United States. A leaf sample was horizontally held above the FFB with the notion of exposing the entire sample to convective heating more evenly. They observed that significant moisture remained in individually tested samples when ignition occurred.

In a natural manzanita shrub stand, leaves display a tendency for a vertical orientation. Prince and Fletcher (2014), Gallacher et al. (2014), Yashwanth et al. (2015), and Gallacher (2016) burned manzanita leaves that were held vertically. Prince and Fletcher (2014) used an FFB for the heating of the leaves and found that leaf edges reached ignition temperatures first. They observed that moisture was present in the live leaves well above 100°C which is water normal boiling point and identified the simultaneous release of water vapor and pyrolysis gases. By investigating the leaf surface temperature, they noted temperature plateaued for moist leaves. This plateau was flatter at lower temperature for the leaf with higher moisture content. In the experiments of Yashwanth et al. (2015) and Gallacher (2016), a radiation panel was included for heating and ignition was found to occur earlier in the combined mode of heating, compared to the cases where the FFB were the source of heating. It is noted that the paper by Yashwanth et al. (2015) was a collaborative work involving both simulation and experimental studies where simulations were conducted by a group at UAH and the experiments by another group at BYU. The simulation results of this work are reviewed later in this section. Gallacher (2016) measured the physical and chemical properties of the foliage from ten live shrub and conifer fuels and burned them throughout a one-year period to investigate the influence of seasons in their burning behavior. Gallacher (2016) also studied the influence of the heating mode on several parameters such as the time required by the leaf to reach 50% of its initial mass, the maximum leaf surface temperature and the leaf plateau temperature. More specifically, he examined three heating modes of convection-only, radiation-only, and combined convection and radiation, and observed that the addition of radiation to convection resulted in faster pyrolysis, higher surface temperature and higher plateau temperature. Moreover, Gallacher (2016) reported that their radiation panel by itself was unable to ignite the leaf. Recently, Safdari et al. (2018, 2019) and Amini et al. (2019) performed experiments to determine what chemicals constitute pyrolysis products of various plant species by heating them using an FFB without burning.

Ignition of wildland fuels has also been studied by experimental setups other than FFB. McAllister and Finney (2017) conducted experiments to investigate autoignition of relatively thick wooden fuels by combined convective and radiative heating. They found that the convective stream temperature has a considerable impact on the ignition location. At a relatively low convective temperature (600°C), the ignition happened in hot spots in the gas phase away from the solid fuel. At a higher convective temperature (800°C), the ignition

occurred very close to the woody fuel glowing tip. Ignition of moist spherical larch wood particles under convection heating was experimentally investigated by Syrodoy et al. (2018). They observed that increasing the gas stream temperature shortened the ignition time, which was an effect more noticeable for particles with larger diameters. Syrodoy et al. (2018) also noted that when the moisture content increased by 20%, ignition time almost doubled. They attributed this significant impact to the relatively large heat of vaporization of water. Lin et al. (2019) investigated the piloted ignition of wooden rods with different diameters and arrangements under radiation heating up to 50 kW/m2. Four fuel diameters ranged from 3.2 to 15.9 mm and three fuel arrangements were examined with a vertical rod, horizontal rod and horizontal bed. They reported that for the single vertical rod, ignition time decreased when the diameter was reduced from 15.9 to 6.4 mm. They also claimed that 3.2 mm fuel rod hardly ignited. They attributed the lacking of igntion to the curvature-enhanced convective cooling, an effect that they claimed to be limited when the single horizontal arrangement was applied.

CFD-based models were also used to simulate the burning of fuels representing individual manzanita leaves (Borujerdi, Shotorban, Mahalingam 2020; Shotorban et al. 2018; Yashwanth et al. 2015, 2016). The main advantage of the CFD-based models are that they can provide a detailed description of thermofluid variables such as the velocity field locally in time and space. Such a description was lacking in the experimental works reviewed above. Yashwanth et al. (2016) investigated the burning of leaf-like fuels under external thermal radiation heating. They modeled the leaf with Gpyro3D (Lautenberger 2014), which was coupled with Fire Dynamics Simulator (FDS) (McGrattan et al. 2013) to represent the flame and gas flow conditions surrounding the leaf. The thermal radiation was supplied by maintaining one of the lateral walls of the computational domain of FDS at 1500 K (equivalent to a heat flux of $\sigma T^4 = 287\mathrm{kW/m^2}$). This termperature was large enough to ignite the modeled fuel. Radiant heat fluxes can be as high as $290\mathrm{kW/m^2}$ according to field-scale measurements of crown fires (Butler et al. 2004). Yashwanth et al. (2016) showed that moisture evaporation and temperature rise took place locally within the fuel and found that ignition occurred on the fuel at a point closer to the heating panel while the regions of the fuel that were far from the radiant heater contained a significant amount of moisture. Yashwanth et al. (2016) assumed for the fuel to be made of cellulose (Bradbury, Sakai, Shafizadeh 1979; Di Blasi 1994). Their modeled fuel thickness (2 mm) was substantially larger than the measured thicknesses reported for manzanita leaves (Pickett et al. 2010). Furthermore, because of the lacking of experimental data for a radiation-only mode of heating, they could not validate their simulations. It is noted that in the experiments, the radiation panel provided a heat flux of 50 $\mathrm{kW/m^2}$ at the sample location which was not high enough to cause ignition (Gallacher 2016). Yashwanth et al. (2015) conducted preliminary simulations, in addition to the experiments reviewed above, for a vertically oriented leaf under convection-only heating and convection-radiation heating. Their simulations used a pyrolysis kinetic model assuming for the modeled fuel to consist of cellulose, lignin and hemicellulose (Manya, Enrique, Puigjaner 2003; Miller and Bellan 1997; Rao and Sharma 1998). Yashwanth et al. (2015) attempted to validate their simulations against the experimental data by comparing the time histories of the measured and simulated fuel mass. However, the validation outcome was a poor match between the modeling and experimental results. This lacking success was mainly attributed to a significant difference between the measured and modeled fuel thicknesses as discussed above. Shotorban et al. (2018) investigated a fuel representing a horizontally oriented manzanita leaf in a computational setup resembling

the experimental setup of Pickett et al. (2010), as reviewed above. They improveded and used Gpyro3D coupled with FDS for simulations. Their modeled fuel thickness was the same as the mean thickness empirically measured for the manzanita leaf. They validated their simulations against the experimental data (Pickett et al. 2010), viz. time histories of normalized mass and mass loss rate, showing a reasonably good match. Their simulations revealed a distinct role that the fluid dynamics plays in moisture evaporation, pyrolysis, ignition, combustion and burnout behavior of leaves. Specifically, they found that the horizontally oriented leaf (with two longer dimensions of the leaf perpendicular to the FFB exit flow) acted as a bluff body in the gas exiting from the FFB. Their simulations further revealed the distinct role that flow structures, e.g., vortices, played in the nonuniform distribution of temperature around the fuel. This effect in turn resulted in a nonuniform release of moisture and pyrolysis gases from the fuel. Consequently, it affected the time and location of ignition and the overall burning behavior. The effect of FMC on the pyrolysis and burning of vertically oriented leaves subject to convective heating was recently studied (Borujerdi et al. 2020) in a computational setup corresponding to the previous measurements (Prince 2014). Four leaf treatments with different FMC values were considered. Simulations revealed that ignition time and critical mass flux increased as FMC increased. It was also shown that while temperature and water vapor distribution around the leaf was substantially affected by the leaf moisture content, the velocity field around the leaf was not appreciably impacted by it.

The present work is a CFD-based modeling study of burning of a vertically oriented leaf subject to three different heating modes: upward convective heating; external thermal radiation heating; and convective heating combined with thermal radiation heating. This work is a significant improvement and extension of a previous modeling attempt as reported in the conference paper (Yashwanth et al. 2015) and reviewed above. The computational model and configuration are reviewed in § 2 and § 3, respectively. Results are shown and discussed in § 4. A summary of the work and conclusions are given in § 5.

Model overview

The modeling study here used a modified version (Shotorban et al. 2018) of Gpyro3D (Lautenberger 2014) coupled with FDS (McGrattan et al. 2013) to represent the thermophysical phenomena in the leaf and the surrounding gas, respectively. Gpyro3D (Lautenberger 2014) treats the solid fuel as a porous medium while accounting for convective and diffusive transport of the gaseous species within the fuel. The conservation equations solved in the modified Gpyro3D (Shotorban et al. 2018) are given and discussed in Appendix A. FDS uses low Mach number approximation for modeling the transport of mass, momentum, energy and chemical species in the gas phase. The equations that are solved in FDS is given in its technical reference (McGrattan et al. 2013). In this study, FDS is set to run in a direct numerical simulation (DNS) mode. When FDS is run in the DNS mode, convective heat flux on a solid surface is directly calculated from difference between the solid surface temperature and the temperature of the gas in the adjacent computational cell. Thermal radiation is accounted for in FDS via a radiation transport equation where gas-phase absorption coefficient is modeled, using a gray-gas assumption. The coupling of Gpyro3D and FDS is achieved by imposing the continuity of temperature, mass fractions, and heat and mass fluxes at the interface of Gpyro3D and FDS domains (Yashwanth et al. 2016).

As the initial condition, the condensed phase in the leaf was assumed to consist of cellulose, hemicellulose, lignin, and liquid moisture while the gas phase within the leaf consisted of standard air (nitrogen and oxygen). Following Prince (2014) who calculated the dry mass composition of the manzanita leaves, using an empirical correlation (Sheng and Azevedo 2002), the dry mass composition was set to 33% cellulose, 33% hemicellulose, and 34% lignin. Recently, Matt et al (2020) who analyzed live leaves from several forest plants (manzanita was not included) reported that in addition to cellulose, hemicellulose and lignin, as some of the main constituents of the leaves, there are significant amounts of protein and lipid. However, their kinetic parameters are not yet known for modeling purposes. The initial liquid moisture mass fraction was specified to be equivalent of 65% FMC on dry basis. This is identical to the FMC of the live leaf burned in the FFB experiment which was used for the validation of the current simulations, as discussed in § 4. Shown in Figure 1 is the generic scheme of the pyrolysis kinetic model used here. It is based on a proposed kinetic model by Miller and Bellan (1997) for dry fuel, and an Arrhenius reaction for moisture vaporization in the moist fuel (Bryden and Hagge 2003; Mell et al. 2009). A comparative study of the Arrhenius approach versus the equilibrium approach for moisture evaporation in biomass has been recently performed with Gpyro (Borujerdi et al. 2019). In this work, char oxidation is not considered, which is a simplification discussed in §4. The kinetic parameters are tabulated in Table 1. Thermophysical properties of the condensed phase species, including heat conductivity, specific heat capacity and density are given in Table 2. Gpyro assumes that all gaseous species have the same diffusion coefficient which is equivalent to the binary diffusion coefficient for diffusion of oxygen into a background species. Here, the background species is nitrogen. To calculate this binary diffusion coefficient, Chapman-Enskog theory is used. The mean porosity of the condensed phase at a given point is obtained through a volumetric averaging defined by Shotorban et al. (2018). In this work, a single step stoichiometric reaction of methane, representative of pyrolysis gases, with air is used to model gas-phase combustion in the FDS domain. The selection of this simple reaction mechanism was partly motivated by a relative success in the validation of the previous modeling work (Shotorban et al. 2018) that used the same mechanism. This simplification seems reasonable considering that the present study is not focused on either a detailed flame structure or pollutant emissions from the flame. Here, an infinitely fast, mixing-controlled combustion model is used for the combustion of methane (McGrattan et al. 2013). Theoretically, fuel and oxidizer cannot simultaneously co-exist outside of a thin reaction sheet in an infinitely fast reaction, which is the default reaction

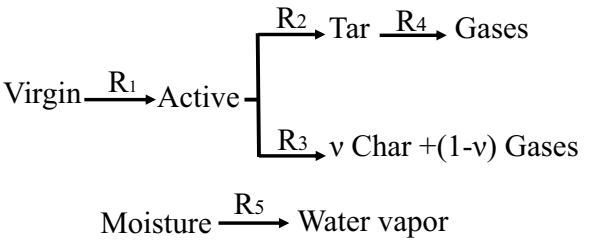

Figure 1. Reaction mechanism for pyrolysis of a dry fuel constituent, viz. cellulose, hemicellulose and lignin (Miller and Bellan 1997), and moisture evaporation (Bryden and Hagge 2003). Kinetic parameters for these reactions are given in Table 1. In reaction R_3, ν is the mass ratio of char formation with values of 0.35, 0.60, and 0.75 for cellulose, hemicellulose and lignin, respectively (Miller and Bellan 1997).

Table 1. Kinetic parameters used for moist fuel (Shotorban et al. 2018) involving pyrolysis reactions $R_1 - R_4$ (Miller and Bellan 1997) and moisture evaporation R_5 (Bryden and Hagge 2003)..

Reaction	$A(s^{-1})$	$E(kJmol^{-1})$	$\Delta h(kJkg^{-1})$
R_1, Cellulose	2.80×10^{19}	242.4	0
R_2, Cellulose	3.28×10^{14}	196.5	225
R_3, Cellulose	1.30×10^{10}	150.5	−20
R_1, Hemicellulose	2.10×10^{16}	186.7	0
R_2, Hemicellulose	8.75×10^{15}	202.4	225
R_3, Hemicellulose	2.60×10^{11}	145.7	−20
R_1, Lignin	9.60×10^{8}	107.6	0
R_2, Lignin	1.50×10^{9}	143.8	225
R_3, Lignin	7.70×10^{6}	111.4	−20
R_4	4.28×10^{6}	108	−42
R_5	5.13×10^{10}	88	2260

Table 2. Thermophysical properties of the moist solid fuel components (Shotorban et al. 2018). In this table, ρ is apparent density, $\hat{\rho}$ is true density, k is thermal conductivity, and c is specific heat capacity. The term "dry fuel" refers to any of cellulose, hemicellulose, and lignin, assumed to have the same thermophysical properties (Miller and Bellan 1997).

Species	$\rho(kgm^{-3})$	$\hat{\rho}(kgm^{-3})$	$k(Wm^{-1}\ K^{-1})$	$c(Jkg^{-1}\ K^{-1})$
Moisture	-	1000	0.596	3900
Dry fuel	650	2167	0.1256	2300
Char	350	2333	0.0837	1100

model in FDS. An extensive discussion on how this is computationally realized in FDS is illustrated by McGrattan et al. (2013). Additionally, it is noted that in the current setup, the gas temperature near the leaf, where the fuel and oxidizer mix, is relatively high (close to 1000 C). As a result, the chemical time scale therein is expected to be small and thus the Damkohler number will be large suggesting the adequacy of the fast chemistry model (Turns 2000).

Computational setup

Figure 2 displays the computational configuration which resembles the reference experimental setup where the burning experiments were performed on freshly harvested manzanita leaves (Gallacher 2016; Gallacher et al. 2014; Yashwanth et al. 2015). Here is an overview of the experimental conditions. Each leaf was held by a cantilever mass balance in a tempered glass duct which prevented ambient air entrainment. One lateral wall of the duct was an Omega QH-101060 radiant panel to provide radiant heating when needed. The radiant heat flux at the sample location was measured 50 kW/m^2. To provide convective heating, an FFB was rolled into a position directly under the leaf and the glass cage. The exhaust gases of the FFB were measured 1000°C and 10 mol% oxygen. A typical manzanita leaf has a face resembling an ellipse with dimensions measured to vary from 0.15 mm to 1.0 mm for thickness; 20 mm to 40 mm for length; and 13 mm to 26 mm for width (Pickett 2008). The mean measured manzanita leaf surface area and mass are $5.62 \pm 0.39cm^2$ and $0.2197 \pm 0.0127g$, respectively (Pickett et al. 2010).

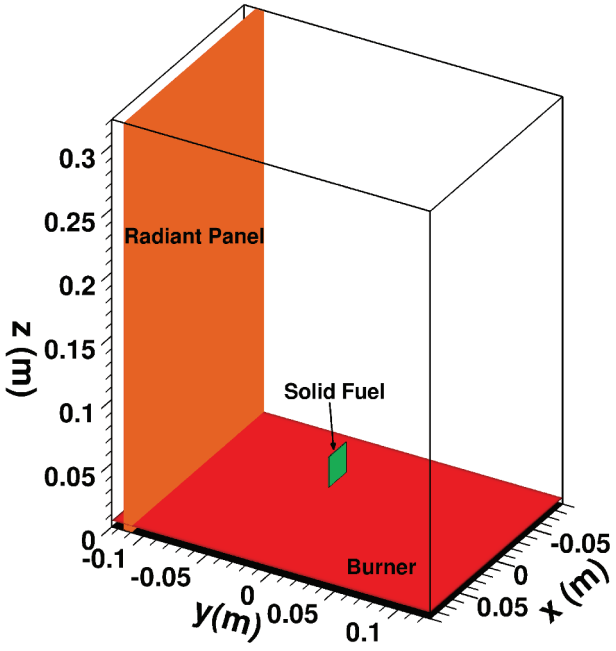

Figure 2. Isometric view of the computational domain with the vertically oriented solid fuel over a flat flame burner equipped with a radiant panel.

The entire computational domain is a rectangular box with dimensions of $0.18 \times 0.25 \times 0.32$ m, which is meshed with a nonuniform grid with resolution of $120 \times 231 \times 216$ cells in x, y and z directions, respectively. It is noted that the central zone of the domain extended from $y = -0.025$ m to $y = 0.025$ m and from $x = -0.09$ m to $x = 0.09$ m has a finer mesh with a computational cell size of $1.50 \times 0.51 \times 1.48$ mm in x, y and z directions, respectively. The rest of the domain has a coarser mesh with a computational cell size of $1.50 \times 1.51 \times 1.48$ mm. Here, the modeled leaf has thickness, length and width of 0.51 mm, 23.7 mm and 23.7 mm, respectively, resulting in the surface area of 5.61cm^2 and a mass of 0.2156g for the leaf (Shotorban et al. 2018). These are within the measured value ranges. Specifically, the thickness is almost in the middle of the range of the measured thickness. The approximation of the leaf face shape by a rectangle is a simplification imposed by the constrain that Gpyro3D is a structured grid-based model with a limitation on dealing with non-rectangular domains. The modeled fuel is meshed with a grid resolution of $48 \times 6 \times 48$ in x, y and z directions, respectively. The center of the solid fuel is located 4 cm above the FFB exit and 11 cm from the radiant panel.

The FFB supplying the convective heating is represented by the bottom surface of the computational domain. This surface has dimensions of 0.18×0.25 m ($x \times y$) through which hot gases enter the domain at 1000°C with 10 mol% oxygen at a velocity of 0.6 m/s, as in BYU experiments (Gallacher 2016; Gallacher et al. 2014; Prince 2014; Yashwanth et al. 2015). The composition of the remaining gases exiting the FFB was not determined in the measurements so they are assumed to be nitrogen (90 mol%) in the simulations. The radiant panel is represented by a vertical heated wall with dimensions of 0.18×0.32 m along x and z. The heated wall temperature is maintained at 952°C throughout the simulation. This provides ~50

kW/m^2 radiation heat flux at the leaf location, which is consistent with the reported radiant heat flux in the reference experiments. Other lateral surfaces of the domain are considered as the solid walls with fixed ambient temperature while the top surface is considered an open boundary.

Results and discussion

Figure 3 shows the time evolution of the normalized fuel mass computed in the current study and measured in the previous BYU experiments (Yashwanth et al. 2015) for the convection-only and combined convection and radiation heating modes. In the experiments, the fuel starts to lose mass slightly sooner, nearly 1 s in the convection-only mode and 0.5 s in the combined mode. The early mass loss is attributed to the leaf water evaporation. Comparing the left and right panels in Figure 3 reveals that as a result of the additional heat flux supplied by the radiant panel, the leaf loses mass faster in the combined mode. The time to reach 50% of the initial mass is determined 7.3 s and 8.1 s for the experiments and the computations, respectively, in the convection-only mode. It is nearly identical and equal to 6.2 s for both experiments and computations in the combined mode. Yearly-averaged time for live manzanita leaves to reach 50% of their initial mass was reported 8.8 s and 5.8 s for convection-only and combined modes, respectively, by Gallacher (2016) who conducted similar burning experiments with the same experimental setup as described above to investigate the seasonal effect. It could be seen in Figure 3 that the simulations slightly underpredict the mass of the fuel remained in the conclusion of the experiments (residual mass). From Figure 3, it could be also understood that in light of the parametric values pertinent to the heating sources, the convective heating seems to have substantially more impact on the pyrolysis and burning process of the leaf than the radiative heating. It takes about 9 s for the leaf to be completely pyrolized when the combined mode is applied. As a result, at the end of ~9 s of combined heating, the leaf loses ~90% of its initial mass. When heating mode is convection-only, as in Figure 3(a), the leaf loses ~60% of its initial mass after 9 s. It is noted that unlike the convection and convection-radiation heating modes, the radiation-only heating mode did not result in ignition in either experiments or computations. The mass versus time was not reported in the previous experiments for this mode. In the computations, it smoothly dropped

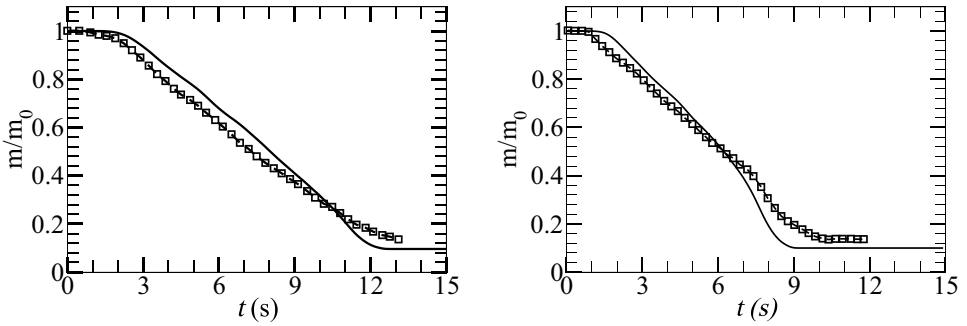

(a) convection-only (b) combined

Figure 3. Time evolution of the leaf mass normalized by the leaf initial mass for heating modes of convection-only and convection combined with radiation in the previous experiments (Yashwanth et al. 2015) (symbolized dashed line) and the current simulations (solid line).

by around 30% by the end 15s, the upper limit of time axis in Figure 3 for the radiation only heating mode. For brevity, the mass was not plotted versus time for this mode.

To investigate the sufficiency of the grid resolution of the solid fuel (48 × 6 × 48), additional simulations were conducted on a finer grid 72 × 6 × 72 and a coarser grid 24 × 3 × 24. When the time evolutions of the normalized mass of the leaf were compared for the three different grids, it was noted that the difference was less than 0.0165 among the normalized masses of the considered grids for the entire time. Also, to investigate the sensitivity of the normalized mass to the resolution in the direction of the leaf thickness, an additional simulation with a grid resolution of 48 × 10 × 48 was performed. The difference between normalized masses of this resolution and the base resolution was found to be less than 0.025 in the entire time.

Further analysis was performed to determine whether fuel is thermally thin or thick. Here,

$$\delta_{\mathrm{T}}(t) = \frac{T(t) - T_0}{|\ T(t)|}, \tag{1}$$

where $\delta_T(t)$ is the thermal zone length scale, was used. Under a one-dimensionality assumption, eq. (1) is simplified to $\delta_{\mathrm{T}} = (T_{\mathrm{s}} - T_0)/(\partial T/\partial x)$ the formulation given by Snegirev, Kuznetsov, and Markus (2017). In eq. (1), $\delta_{\mathrm{T}}(t)$ was calculated, using the temperature data available at fuel grid points at various time steps. It was confirmed that away from the fuel edges, this equation simplifies to Snegirev et al.'s formulation. Further, data visualization was conducted with the condition $\delta_{\mathrm{T}} > 0.25$mm (∼ the fuel half thickness) and realized that, this condition was satisfied all the time except for an initial time period of $t < 1$s. This finding suggests that except for the first second, the fuel may be considered thermally thin. Hence, the divergence of the heat flux in the energy eq. (A.3) may be negligible for the setup studied here. Moreover, it was determined that δ_{T} was never smaller than the grid size 0.102 mm. Determining whether the fuel is chemically thin or thick would be also of interest (Snegirev, Kuznetsov, Markus 2017). However, the available Zeldovich number-based approach (Snegirev, Kuznetsov, Markus 2017) for doing so relies on critical assumptions including one-step pyrolysis reaction (only one chemical time scale), which is not the case here.

Another grid resolution was also examined for the gas domain where the grid size was doubled in the x and z directions. The grid size in the y direction did not change as it had to stay identical to the fuel thickness. The difference between the leaf normalized masses in the simulations with this resolution and the base resolution described in § 3, was noted to be less than 0.048 in all simulation time.

Figure 4 displays the time evolution of the fuel normalized mass loss rate (MLR) in the current model and the previous BYU experiments (Yashwanth et al. 2015) for the convection-only and combined convection and radiation heating modes. The computed and measured MLRs exhibit a similar behavior over time. The MLRs start off with a zero value at time zero. Initially, the leaf does not loss much of mass but mainly heats up. Later, at the onset of water evaporation, MLR starts gaining appreciable values. There exists a major peak value early in the process which is mainly attributable to the moisture evaporation. After a while, when the fuel element reaches sufficiently high temperatures, pyrolysis commences and contributes to the mass loss as well. Formation of the flame around the leaf provides additional heating to the leaf, accelerating the fuel degradation. When the leaf is mostly converted to the char and the pyrolysis

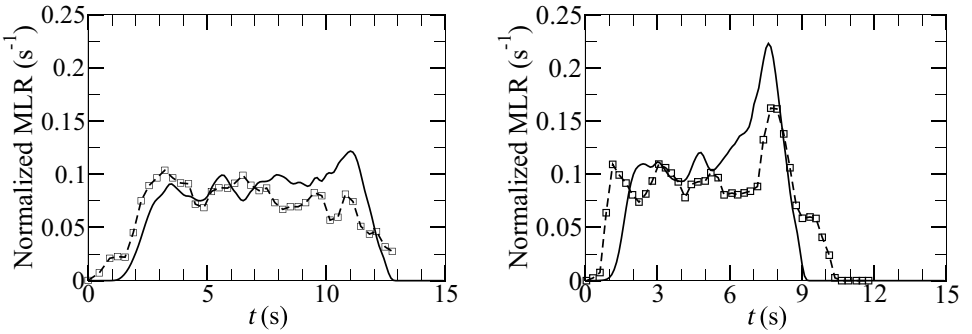

(a) convection-only (b) combined

Figure 4. Time evolution of the solid fuel normalized mass loss rate for the heating modes of convection-only and convection combined with radiation in the previous experiments (Yashwanth et al. 2015) (symbolized dashed line) and the current simulations (solid line).

slows down, MLR exhibits a drastic drop at about 11 s in the convection-only mode and 7.6 s in the combined mode. The MLR eventually diminish by the completion of the pyrolysis process. Since in the case of the combined heating mode, the rate of heat transfer to the fuel element is higher, the MLR exhibits overall higher values and the degradation of the leaf ends 3.6 s sooner. For the radiation-only mode (not shown in Figure 4), MLR values are relatively very small since the leaf receives substantially less heat flux compared to the other two heating modes.

In Figure 5, the heat release rate (HRR), i.e. the rate of heat generation by the combustion of gaseous fuel in FDS, is plotted against time. As seen in this figure, HRR starts to gain appreciable values after ~3 s and ~2.7 s for the convection-only and combined convection and radiation modes, respectively. The first noticeable peaks at ~3.4 s and ~3.0 s for convection-only and combined modes, respectively, are attributed to the ignition. The ignition occurs sooner for the combined mode as the overall rate of heat transfer to the leaf is higher. Note that ignition takes place around the times at which the MLR achieves its first major peak (see Figure 4). The previous experiments (Yashwanth et al. 2015) reported ignition time of 3.1 s for the convection-only mode, noting that the time at which a visual flame is formed was identified as the ignition time in the experiments. It is also seen in Figure 5 that after ignition, the HRR increases for a while for both heating modes but with a higher rate for the combined mode. This rise takes place during a time interval when the flame is formed and grows while the gaseous fuel is released as a result of solid fuel devolatilization. The HRR peak value is higher but the peak time is smaller in the combined mode of heating, compared to the convective-only mode. After reaching the peak, HRR exhibits a relatively sharp drop as the solid fuel has been mostly transformed to the char and thus the pyrolysis process slows down. This behavior is consistent with the drop of MLR seen in Figure 4. Consequently, the mass flow rate of the gaseous fuel into the gas domain decreases and the flame extinction stage begins (Tihay et al. 2009). The flame extinguishes at times ~12.7 s and ~9.1 s for convection-only and combined convection and radiation modes, respectively, as could be seen in Figure 5. The overall amount of heat released by combustion is calculated 443.7 J and 436.4 J for the convection-only mode and the combined mode, respectively, which differ by less than 2%. This consistency shows that although the addition of a radiant panel increases the HRR initially, it has little impact on the overall heat release by combustion. The reason is that the an identical solid fuel is used for both modes of

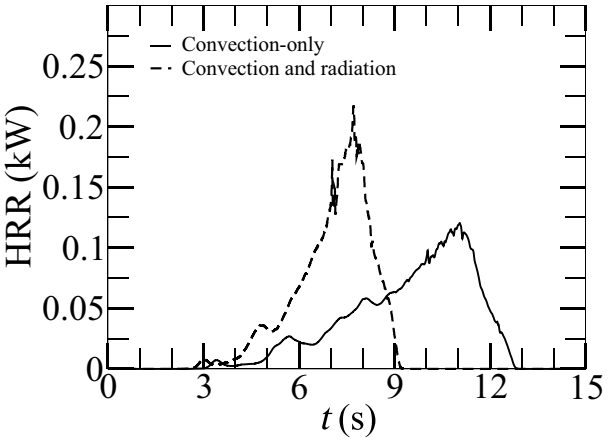

Figure 5. Time history of heat release rate.

heating. The computed HRR is zero when the heating mode is radiation-only since no ignition or flame is formed for this mode. For remaining of this section, the results are presented for convection-only and combined heating modes in which ignition and flaming occur.

Figure 6 displays solid fuel temperature profiles along x, on $y = 0$ plane, for three H values and at two time instances of $t = 6$s and $t = 8$s for both heating modes. Note that $H = z - 28.15$mm and thus H is the vertical distance measured from the leaf leading (bottom) edge. Note that the fuel element spans 0.0237m in both x and z directions. The panels in this figure indicate the heating patterns of the solid fuel: It is heated up from the bottom to the top and from the edges inward. The bottom part of the fuel is the closest to the burner. When the hot gases meet the fuel at this part, boundary layers over the fuel faces are formed. Consequently, the heat transfer rate from the hot gas stream to the solid fuel decreases along the flow (z) direction. Within the leaf, heat from the hotter edges is transferred inward by means of conduction, heating up its interior regions. The other factor affecting temperature distribution in the solid fuel is the location of the reaction zone for gases outside of the fuel. This effect is clearly illustrated in Figure 6(d) where the leaf temperature around the edges is higher for an upper location. The reason for this behavior is that at the time associated with this figure, a flame exists in the vicinity of the downstream part of the fuel which further heats up the fuel therein. Comparing left panels to right panels in Figure 6 indicates that the radiant panel significantly accelerates the heating of fuel.

Figure 7 shows contours of the water mass fraction in the fuel on an xz slice passing through $y = 0$ plane (the mid-plane of the fuel) at three different times for both heating modes. A drying front propagating from the sides to the center is visible in this figure. The drying front divides the slice into two zones: the dry zone and the wet zone (Galgano and Di Blasi 2004; Saastamoinen 1993) such that while the former expands in time, the latter shrinks and eventually vanishes. Overall, the spatial distribution of water in the leaf is consistent with the temperature distribution. In other words, the edges of the leaf reach higher evaporation rates since they gain higher temperatures more rapidly compared to the innermost regions of the leaf. A similar observation was made in the previous related experiments (Gallacher 2016; Prince 2014; Prince and Fletcher 2014), as reviewed in § 1. Another finding, consistent with the observations in previous experiments, was that the leaf

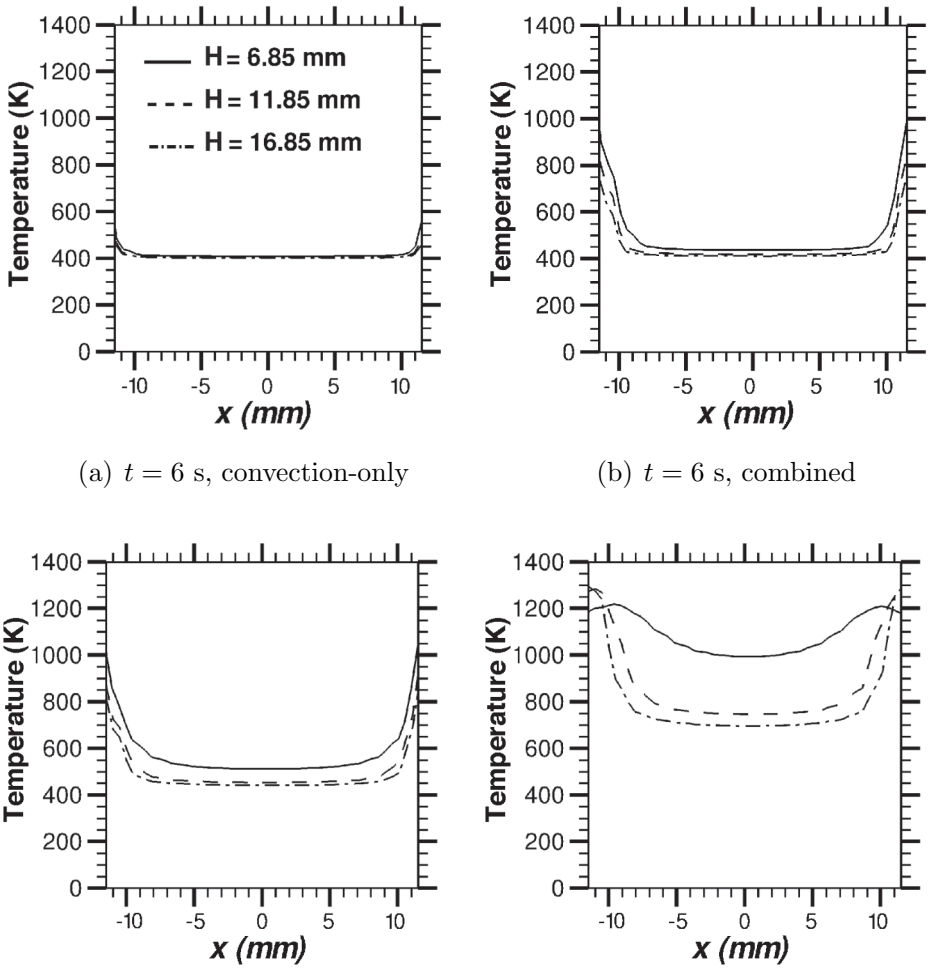

(a) $t = 6$ s, convection-only (b) $t = 6$ s, combined

(c) $t = 8$ s, convection-only (d) $t = 8$ s, combined

Figure 6. Solid fuel temperature versus x on the mid-plane $y = 0$ at $t = 6$ and 8s in convection-only and combined convection and radiation heating.

still contains considerable amount of liquid moisture after ignition. Figure 7(b,e) can exemplify this finding, noting that ignition occurs at $t = 3.3$s and 3.0s for convection-only and combined convection and radiation modes, respectively. The lower corners of the leaf are the first parts of the leaf that dry. These are the parts where the ignition occurs, as will be discussed later. As could be seen in this figure, the leaf loses moisture more rapidly in the case of combined heating mode.

Figure 8 displays temperature, vertical velocity, and oxygen volume fraction in the gas (FDS) domain versus y, at $z = 0.045$m and $x = 0$m, and at $t = 10$s and $t = 6$s for the convection-only (upper panels) and combined (lower panels) heating mode, respectively. These specific times are selected since they correspond to instances when the flame has developed well and thus its effect on the gas phase near the leaf can be shown more

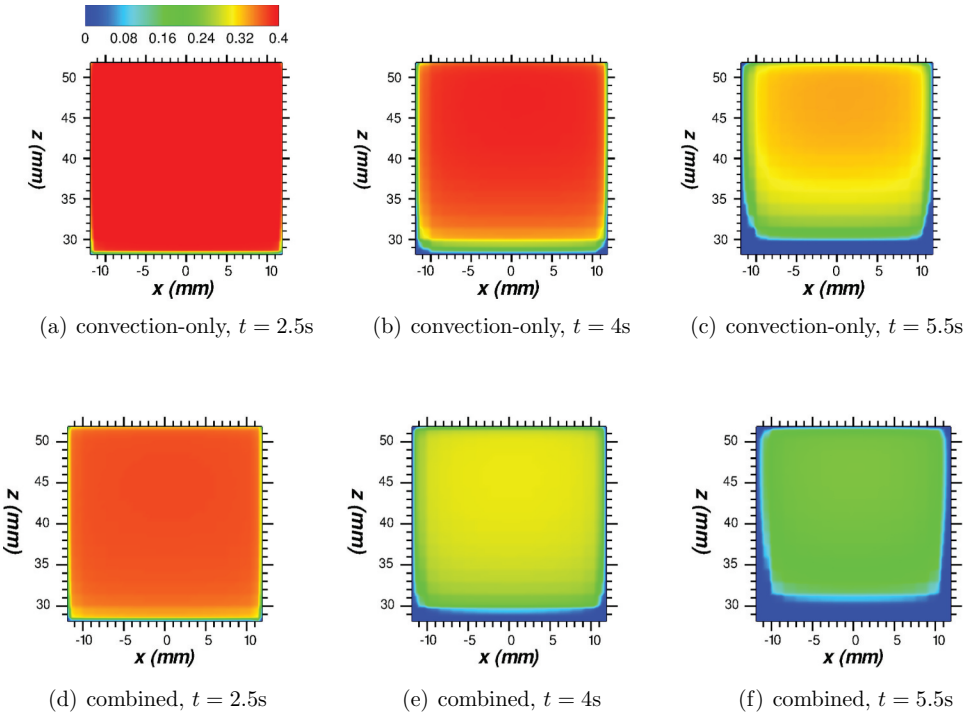

(a) convection-only, $t = 2.5$s (b) convection-only, $t = 4$s (c) convection-only, $t = 5.5$s

(d) combined, $t = 2.5$s (e) combined, $t = 4$s (f) combined, $t = 5.5$s

Figure 7. Contours of the liquid moisture mass fraction in solid fuel at $t = 2.5$, 4 and 5.5s on an *xz* slice at $y = 0$ for the heating modes of convection-only and combined convection and radiation.

distinctly. Note that the solid fuel extends from $y = -0.25$mm to $y = 0.25$mm. The vertical stripe in middle has a thickness identical to the thickness of the fuel. The formation of momentum, thermal, and concentration boundary layers on the lateral faces of the leaf is evident in this figure. The followings are the discussions made with respect to the left face and similar discussions could be made with respect to the right face. Seen in Figure 8(a,d) is that the gas temperature increases with the distance from the leaf face, reaching a peak value and then gradually dropping to plateau at 1000°C, which is the temperature of the gases at the FFB exit. Temperature rises above this value since there is a flame at the times associated with Figure 8. If there were no flame, the gas temperature would monotonically rise to 1000°C with the distance from the leaf face. It is understood from Figure 8(b,e) that the vertical velocity is zero at the fuel face which is due to the no slip condition. Immediately off the face, the gas flow gains positive vertical velocity values due to the freestream originated from the FFB. Because of the flame, gas is heated up and the velocity additionally rises. It is shown in Figure 8(c,f) that the volume fraction of oxygen decreases as the distance to the leaf decreases. This decrease is attributed to two interacting phenomena. First, the evaporated moisture from the leaf displaces oxygen away from the leaf. Second, the oxygen is consumed in the combustion reaction zone. Away from the leaf, the volume fraction of oxygen plateaus to 0.1, identical to the volume fraction of oxygen at the FFB exit.

While the profiles of gas temperature and vertical velocity, and oxygen volume fraction exhibit a symmetry on two sides of the leaf as a result of symmetric heating in the convection-only mode, the spatial distributions of those variables exhibit an asymmetry

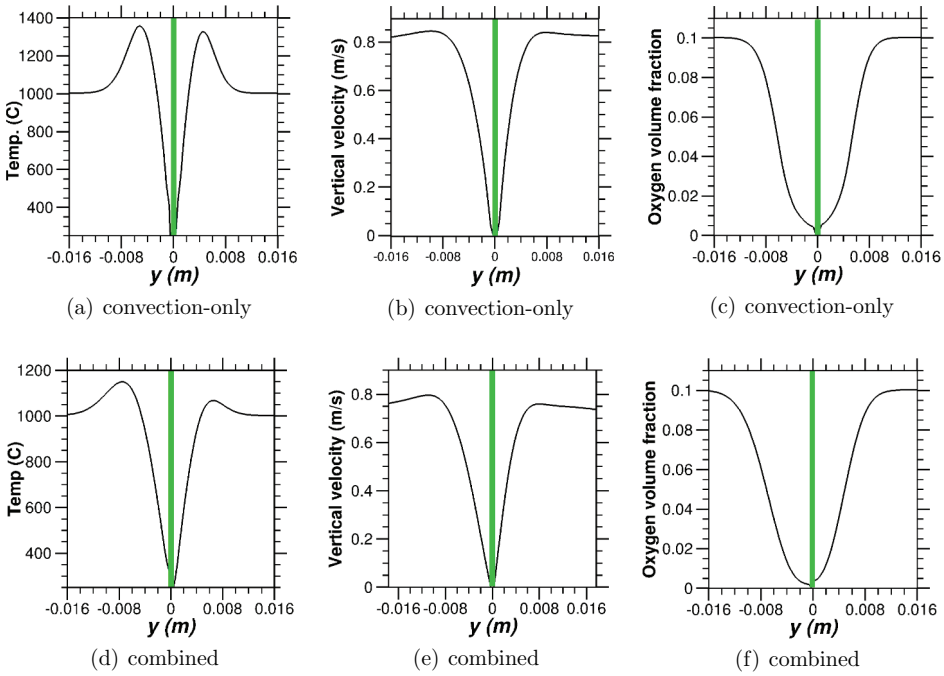

Figure 8. Temperature, vertical (z-component) velocity and oxygen volume fraction versus y at $x = 0$m and $z = 0.045$m in the gas phase domain near the leaf at $t = 10$s for the convection-only heating mode and $t = 6$s for the combined heating mode. The thick line in the middle indicates the leaf span in y direction.

with respect to the leaf faces in the combined mode. The reason for this asymmetric behavior is that the left face of the leaf is opposite to the radiant panel. Hence, the left face heats up faster than the right face and the physical and thermochemical processes lag on the right side of the leaf. For instance, referring to Figure 8(d), the gas temperature peak on the left side is ~1150°C which is about 75°C higher than that on the right side and indicates that the combustion reaction rate is higher on the left side. As a result, oxygen is consumed faster and has overall lower amount in the left side as can be seen in Figure 8(f). Moreover, as shown in Figure 8(e), the peak of the vertical velocity which occurs in the reaction zone, is higher on the left side of the leaf mostly because the peak temperature is higher therein compared to that on the right side.

The following analysis evaluates the adequacy of FDS grid resolution in the direction normal to the leaf face. Rouvreau et al. (2002) studied diffusion flames in the laminar boundary layer using FDS with infinitely fast chemistry. Therein, in a setup similar to the flame-flow study here, gaseous fuel was injected from a $6 \times 6\,\mathrm{cm}^2$ plane, perpendicular to the oxidizer flow in a $30 \times 20 \times 15\,\mathrm{cm}^3$ box. When there was a flame, Rouvreau et al. (2002) examined the velocity overshoot $\tilde{w} = w/U$, where w and U were the velocity parallel to the wall and the free stream velocity, respectively. They reported that the velocity overshoot can be as high as 1.35. Hence, one can conclude that due to flame, the velocity in the boundary layer could be 135% of the free stream velocity. In Figure 8(b), $\tilde{w}$ is 1.46, which is consistent with the findings of Rouvreau et al. (2002). Further, the grid size in the direction normal to the wall was 2 mm in this reference,

where they showed a good match between numerical results and the experimental flame temperature and shape. Therein, the flame width was calculated ~20 mm, indicating that 10 grid points were used across it. Here, the flame width is ~10 mm and the grid size is 0.5 mm, indicating that 20 grid points were used to resolve the flame in the direction normal to the wall. Hence, the grid resolution in this direction seems reasonable.

Figure 9 displays the combustion heat release rate per unit volume (HRRPUV) versus z in FDS at the intersection of $x = 0$m and $y = -0.0025$m planes which is located on the left side of the leaf. The shown z range extends from the leading edge to the trailing edge of the leaf. As seen in Figure 9(a), in the case of convection-only heating mode, as time elapses from $t = 6$s to $t = 9$s, the flame propagates upward and the combustion process generates more heat. This is demonstrated by the fact that as time passes, the peak in HRRPUV shifts upward and also the area under HRRPUV which correlates with the heat generation, increases. In contrast, in the combined heating mode, while the flame propagates upward with time, the heat generation by combustion reduces over the vertical line considered here. This observation is justified by the fact that in the case of combined mode, the flame extinguishes earlier.

Figure 10 shows contour plots of temperature, and oxygen and water vapor volume fractions in the FDS domain on a yz slice passing through $x = 0$ plane for the convection-only mode at two different times $t = 3$s (first row) and $t = 11$s (second row), and for the combined mode at $t = 7.5$s (third row). Note that $t = 3$s corresponds to an instance before ignition while $t = 11$s and $t = 7.5$s represent after ignition instances when the leaf MLR experiences its peak for each heating mode as shown in Figure 4. At all times shown here, in the region where the leaf is located, the flow pattern is mainly dictated by the boundary layers (Also, see Figure 8). Figure 10 (a) shows that at time 3 s, no flame is formed and the fuel element is heated up by convection heat transfer through the boundary layers as well as conduction heat transfer within the fuel. The

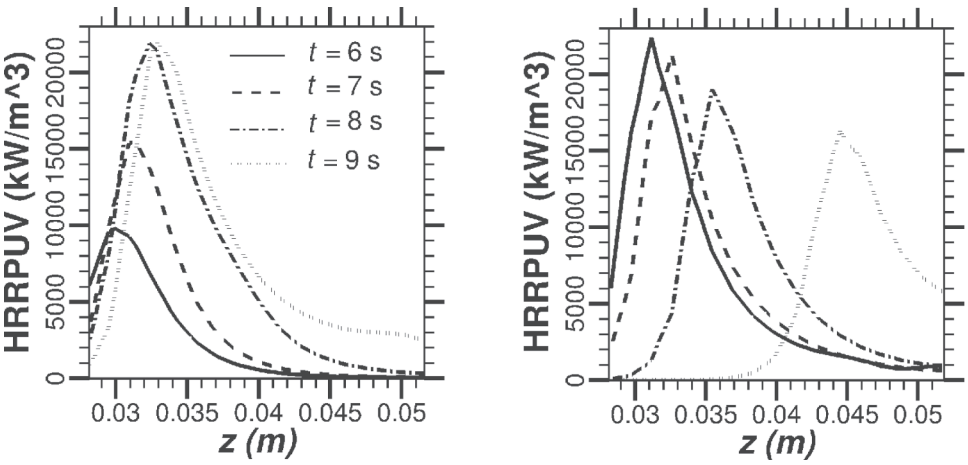

(a) convection-only (b) combined

Figure 9. Heat release rate per unit volume (HRRPUV) versus z at $x = 0$m (the central yz plane) and $y = -0.0025$m in the gas phase domain at four consecutive times for convection-only and combined heating modes. In the shown range of z, it extends from the leading edge to the trailing edge of the leaf. The locations examined here have a horizontal distance of 2.25 mm from the left face of the leaf, located between the left face and the radiant panel.

water vapor resulting from the moisture evaporation is transferred outside of the fuel as evident in Figure 10(c). As the water vapor is released from the fuel, it displaces the oxygen around the fuel. Hence, oxygen concentration is reduced in this region, as seen in Figure 10(b). Furthermore, the release of water vapor into the surrounding, influences the thermal boundary layer, and consequently the heat transfer therein. At post-ignition times, i.e. 11 s and 7.5 s as could be seen in Figure 10(d,g), there is a flame characterized by a high-temperature reaction zone. The exothermic oxidation of the fuel vapor released from the solid fuel occurs in this zone. Consequently, oxygen is consumed by combustion and its concentration decreases there as evident in Figure 10(e,h). On the other hand, water vapor is produced by the combustion reaction in this zone, as seen in Figure 10(f,i). It is noted that at $t = 11$s and $t = 11$s all of the liquid moisture in the leaf has been already vaporized and thus at all water vapor around the leaf is due to combustion not water vaporization. At the times considered here for the combined

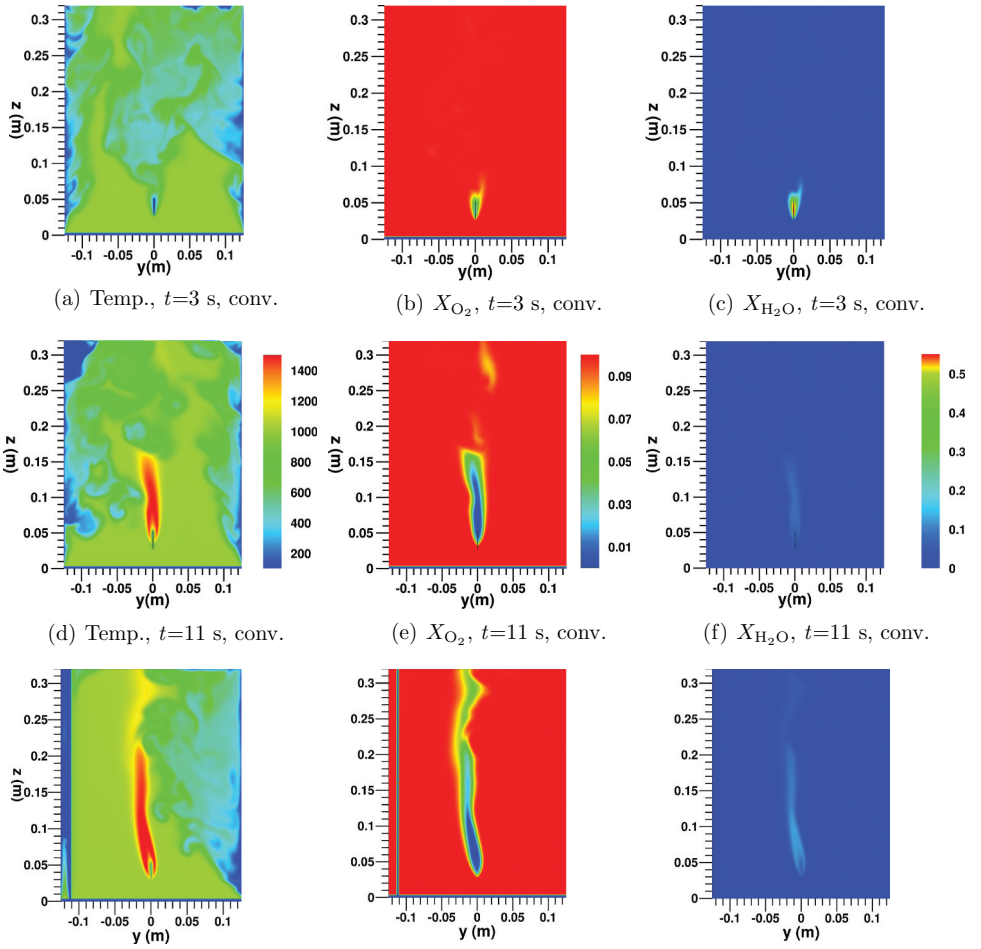

(a) Temp., t=3 s, conv. (b) X_{O_2}, t=3 s, conv. (c) X_{H_2O}, t=3 s, conv.

(d) Temp., t=11 s, conv. (e) X_{O_2}, t=11 s, conv. (f) X_{H_2O}, t=11 s, conv.

(g) Temp., t=7.5 s, combined (h) X_{O_2}, t=7.5 s, combined (i) X_{H_2O}, t=7.5 s, combined

Figure 10. Contours of temperature (in °C), and oxygen and water vapor volume fractions in the gas domain for the convection-only heating mode at $t = 3$s (before ignition) and 11s (after ignition at the peak of MLR), and the combined heating mode at $t = 7.5$s (after ignition at the peak of MLR).

mode, the leaf achieves higher MLR since compared to the convection-only mode, gaseous fuel is released faster. This is the main reason for a relatively larger flame in the combined mode.

Contour plots of Figure 10(b,e,h) help justify the neglect of char oxidation here. Char oxidation is very dependent on the oxygen mass transfer to the solid fuel surface (Chaos, Khan, Dorofeev et al. 2013). As shown in Figure 10(b), during the pyrolysis, water vapor and pyrolysis gases displace the oxygen away from the leaf, acting as a barrier against oxygen diffusion to the leaf. In the flaming stage, as shown in Figure 10(e,h), oxygen is primarily consumed in the combustion reaction and hence the amount of oxygen around the leaf is further reduced. Char oxidation may take place upstream of the flame where oxygen is not rare. However, Burrows (2001) who experimentally investigated burning of different kinds of wildland fuels, observed that for leaves, the contribution of the flaming combustion to the leaf mass loss is much larger than the contribution of the char oxidation. The flame propagation pattern, described by examining temperature contours at two times shown in Figure 10(a,d) and other intermediate times not shown here, looks qualitatively consistent with the pattern observed in the previous experiments on live manzanita leaves (Prince 2014).

Figure 11 displays iso-surfaces of HRR per unit volume of $15\mathrm{kWm}^{-3}$ at four different times after ignition for convection-only mode. Figure 11(a) shows that ignition occurs at the lower corners of the leaf. These spots are adjacent to where the leaf is heated up, dried and pyrolyzed more rapidly than the rest of the fuel. These parts of the leaf belong to the closest region of the leaf to the burner while having locally more areas exposed to hot gases and hence, receiving higher local heat. After 2 s, as seen in Figure 11(b), the flame grows along the leading (bottom) edge and then at the later times, the flame continues growing and propagating upward as seen inFigure 11(c,d).

Summary and conclusions

Pyrolysis and combustion of a solid fuel element representing a live manzanita leaf was computationally investigated under various heating modes prevalent in wildland fires. The computational setup mimicked a bench top scale experimental apparatus previously used to burn vertically oriented live manzanita leaves. The leaf was oriented vertically and subjected to an upward convection of hot gases exiting a flat flame burner (FFB) with a temperature of 1000°C, and oxygen of 10 mol% and minimal thermal radiation. In the combined convection-radiation heating mode, in addition to this convection mechanism, a radiant panel, installed in parallel and opposite to one of the leaf faces, used to provide radiative heating. In the radiation-only mode, only the radiant panel operated. A modified version of Gpyro3D coupled with FDS was used for computations.

Time histories of the normalized mass and mass loss rate of the leaf were found in a good agreement with the previous experimental data in the convection-only and combined heating modes. Time history of the heat release rate revealed that the ignition time in the computations was ~3.4 s and ~3.0 s for the convection-only and combined modes, respectively. These values were consistent with the ignition times reported in the corresponding previous experiments. The overall heat release by combustion was almost identical in both modes. For the radiation-only mode, simulations showed no ignition, a finding consistent with the observations in the previous radiation-only experiments for a similar applied radiative heat flux. No experimental mass evolution data was reported for this mode. Hence, no validation was performed for computations in the radiation-only mode.

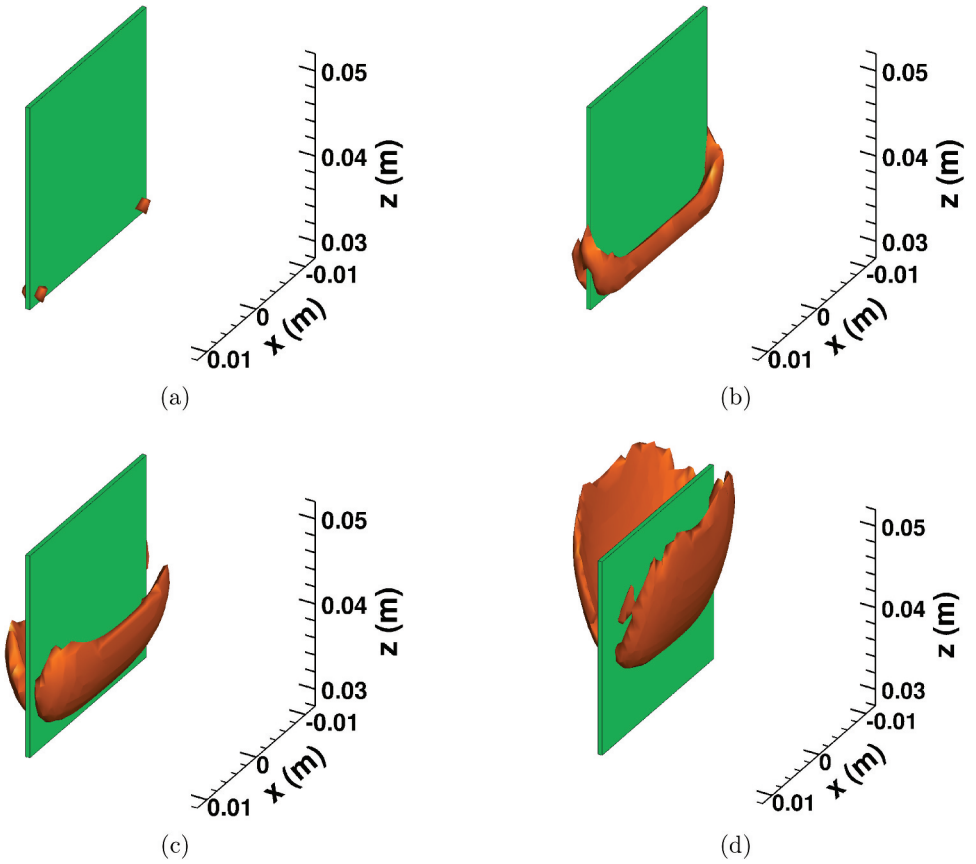

Figure 11. Iso-surfaces of heat release rate per unit volume of 15kWm^{-3} at (a) $t = 5$s; (b) $t = 7$s; (c) $t = 9$s; and (d) $t = 11$s for convection-only mode.

The simulations furthered the knowledge gained in the previous relevant experiments as the response of the leaf to various heating modes was investigated by shedding light on the role of spatial and temporal variation of flow variables such as temperature, velocity and heat release rate in pyrolysis, ignition, flaming and overall burning behavior of the leaf. They revealed the boundary layers formed on the leaf faces, which played a critical role in heating and thermo-chemical conversion of the leaf. This fluid dynamical effect was completely different from that in the horizontally oriented leaves, as illustrated in the previous simulations (Shotorban et al. 2018). Therein, the fuel acted as a bluff body with a stagnation point formed on the leaf face against the hot gas flow of the FFB and the vorticies formed near the other face. Moreover, it was shown that in the combined mode of heating, where one of the leaf faces was exposed to the radiation panel, boundary layers formed on the faces of the leaf were asymmetric and so was the distribution of the flow variables around the leaf. In the convection-only mode, those variables showed a near-perfect symmetry on both sides of the leaf. Additional analysis revealed that except for the fist second, the fuel may be considered thermally thin.

Contours of the liquid moisture mass fraction showed that there was an evaporation front within the leaf which propagated from the edges inward while dividing the fuel domain into dry and wet zones. Before ignition, the water vapor that was originated from moisture

evaporation in the solid fuel, was released into the gas phase surrounding the leaf. As a result, oxygen was somewhat displaced and its volume fraction was reduced near the solid fuel. After ignition, combustion of the pyrolysis gas substantially decreased oxygen concentration in this zone and produced water vapor around and above the leaf. It was noted that the addition of the radiation panel caused the gaseous fuel to be released with higher rates. As a result, the flame zone was larger in the combined mode of heating, compared to the convection-only mode. Iso-surfaces of heat release rate per unit volume showed that ignition occurred near the lower corners of the leaf which was heated up, lost moisture and pyrolyezed more rapidly than the rest of the leaf. This effect was the outcome of the fact that these corners received the highest heating rates in both heating modes, compared to the rest of the leaf. It was illustrated with iso-surface snapshots of the heat release rate per unit volume that after ignition, the flame first grew over the leaf leading edge, and then developed and moved up over the leaf faces in a pattern mainly dominated by the boundary layers.

Acknowledgments

This work was supported by DOD/EPA/DOE Strategic Environmental Research and Development Program project RC-2640 administered by the USDA Forest Service PSW Research Station through cooperative agreement JV-11272167-025 with The University of Alabama in Huntsville. The authors appreciate the useful discussions with Shankar Mahalingam of UAH, Chris Lautenberger of Reax Engineering, Thomas H. Fletcher of BYU and David R. Weise of USDAFS.

Funding

This work was supported by the Strategic Environmental Research and Development Program [RC-2640]; USDA Forest Service [JV-11272167-025].

ORCID

Babak Shotorban http://orcid.org/0000-0001-6838-7297

References

Amini, E., M.-S. Safdari, J. T. DeYoung, D. R. Weise, and T. H. Fletcher. 2019. Characterization of pyrolysis products from slow pyrolysis of live and dead vegetation native to the southern united states. *Fuel* 235:1475–91. doi:10.1016/j.fuel.2018.08.112.

Borujerdi, P. R., B. Shotorban, and S. Mahalingam. 2020. A computational study of burning of vertically oriented leaves with various fuel moisture contents by upward convective heating. *Fuel* 276:118030. doi:10.1016/j.fuel.2020.118030.

Borujerdi, P. R., B. Shotorban, S. Mahalingam, and D. R. Weise. 2019. Modeling of water evaporation from a shrinking moist biomass slab subject to heating: Arrhenius approach versus equilibrium approach. *Int. J. Heat Mass Transf.* 145:118672. doi:10.1016/j.ijheatmasstransfer.2019.118672.

Bradbury, A. G. W., Y. Sakai, and F. Shafizadeh. 1979. A kinetic model for pyrolysis of cellulose. *J. Appl. Polym. Sci.* 23 (11):3271–80. doi:10.1002/app.1979.070231112.

Bryden, K. M., and M. J. Hagge. 2003. Modeling the combined impact of moisture and char shrinkage on the pyrolysis of a biomass particle. *Fuel* 82 (13):1633–44. doi:10.1016/S0016-2361(03)00108-X.

Burrows, N. D. 2001. Flame residence times and rates of weight loss of eucalypt forest fuel particles. *Int. J. Wildland Fire* 10 (2):137–43. doi:10.1071/WF01005.

Butler, B., J. Cohen, D. Latham, R. Schuette, P. Sopko, K. Shannon, D. Jimenez, and L. Bradshaw. 2004. Measurements of radiant emissive power and temperatures in crown fires. *Can. J. For. Res.* 34 (8):1577–87. doi:10.1139/x04-060.

Chaos, M., M. M. Khan, and S. B. Dorofeev. 2013. Pyrolysis of corrugated cardboard in inert and oxidative environments. *Proc. Combust. Inst.* 34 (2):2583–90. doi:10.1016/j.proci.2012.06.031.

Di Blasi, C. 1994. Numerical simulation of cellulose pyrolysis. *Biomass Bioenergy* 7 ((1–6)):87–98. doi:10.1016/0961-9534(94)00040-Z.

Engstrom, J., J. Butler, S. Smith, L. Baxter, T. Fletcher, and D. Weise. 2004. Ignition behavior of live california chaparral leaves. *Combust. Sci. Technol.* 176 (9):1577–91. doi:10.1080/00102200490474278.

Galgano, A., and C. Di Blasi. 2004. Modeling the propagation of drying and decomposition fronts in wood. *Combust. Flame* 139 (1–2):16–27. doi:10.1016/j.combustflame.2004.07.004.

Gallacher, J. R. (2016), The influence of season, heating mode and slope angle on wildland fire behavior, PhD dissertation, Brigham Young University, Provo, UT.

Gallacher, J. R., V. Lansinger, S. Hansen, D. Jack, D. R. Weise, and T. H. Fletcher (2014), Effects of season and heating mode on ignition and burning behavior of three species of live fuel measured in a flat-flame burner system, *in* 'Spring Technical Meeting of the Western States Section of the Combustion Institute', Pasadena, CA.

Lautenberger, C. (2014), Gpyro–a generalized pyrolysis model for combustible solids, Technical Reference Version 0.8, Reax Engineering Inc., Berkeley, CA.

Li, J., S. Mahalingam, and D. R. Weise. 2017. Experimental investigation of fire propagation in single live shrubs. *Int. J. Wildland Fire* 26 (1):58–70. doi:10.1071/WF16042.

Lin, S., X. Huang, J. Urban, S. McAllister, and C. Fernandez-Pello. 2019. Piloted ignition of cylindrical wildland fuels under irradiation. front. *Mech. Eng.* 5:54.

Manya, J. J., V. Enrique, and L. Puigjaner. 2003. Kinetics of biomass pyrolysis: A reformulated three-parallel-reactions model. *Ind. Eng. Chem. Res.* 42 (3):434–41. doi:10.1021/ie020218p.

Matt, F. J., M. A. Dietenberger, and D. R. Weise. 2020. Summative and ultimate analysis of live leaves from southern us forest plants for use in fire modeling. *Energ. Fuel.* 34 (4):4703–20. doi:10.1021/acs.energyfuels.9b04107.

McAllister, S., and M. Finney. 2017. Autoignition of wood under combined convective and radiative heating. *Proc. Combust. Inst.* 36 (2):3073–80. doi:10.1016/j.proci.2016.06.110.

McGrattan, K., S. Hostikka, R. McDermott, J. Floyd, C. Weinschenk, and K. Overholt (2013), Fire Dynamics Simulator technical reference guide Volume 1: Mathematical model, Special Publication 1018–6, U.S. Department of Commerce, National Institute of Standards and Technology.

Mell, W., A. Maranghides, R. McDermott, and S. L. Manzello. 2009. Numerical simulation and experiments of burning douglas fir trees. *Combust. Flame* 156 (10):2023–41. doi:10.1016/j.combustflame.2009.06.015.

Miller, R. S., and J. Bellan. 1997. A generalized biomass pyrolysis model based on superimposed cellulose, hemicelluloseand lignin kinetics. *Combust. Sci. Technol* 126 (1–6):97–137. doi:10.1080/00102209708935670.

Pickett, B. M. (2008), Effects of moisture on combustion of live wildland forest fuels, PhD dissertation, Brigham Young University, Provo, UT.

Pickett, B. M., C. Isackson, R. Wunder, T. H. Fletcher, B. W. Butler, and D. R. Weise. 2010. Experimental measurements during combustion of moist individual foliage samples. *Int. J. Wildland Fire* 19 (2):153–62. doi:10.1071/WF07121.

Prince, D., C. Shen, and T. Fletcher. 2017. Semi-empirical model for fire spread in shrubs with spatially-defined fuel elements and flames. *Fire Technol.* 53 (3):1439–69. doi:10.1007/s10694-016-0644-9.

Prince, D. R. (2014), Measurement and modeling of fire behavior in leaves and sparse shrubs, PhD dissertation, Brigham Young University, Provo, UT.

Prince, D. R., and T. H. Fletcher. 2014. Differences in burning behavior of live and dead leaves, Part 1: Measurements. *Combust. Sci. Technol.* 186 (12):1844–57. doi:10.1080/00102202.2014.923412.

Rao, T. R., and A. Sharma. 1998. Pyrolysis rates of biomass materials. *Energy* 23 (11):973–78. doi:10.1016/S0360-5442(98)00037-1.

Rouvreau, S., P. Joulain, H. Y. Wang, P. Cordeiro, and J. L. Torero. 2002. Numerical evaluation of boundary-layer assumptions used for the prediction of the standoff distance of a laminar diffusion flame. *Proc. Combust. Inst.* 29 (2):2527–34. doi:10.1016/S1540-7489(02)80308-X.

Saastamoinen, J. (1993), Model for drying and pyrolysis in an updraft biomass gasifier, *in* 'Advances in thermochemical biomass conversion', Springer, pp. 186–200.

Safdari, M.-S., E. Amini, D. R. Weise, and T. H. Fletcher. 2019. Heating rate and temperature effects on pyrolysis products from live wildland fuels. *Fuel* 242:295–304. doi:10.1016/j.fuel.2019.01.040.

Safdari, M.-S., M. Rahmati, E. Amini, J. E. Howarth, J. P. Berryhill, M. Dietenberger, D. R. Weise, and T. H. Fletcher. 2018. Characterization of pyrolysis products from fast pyrolysis of live and dead vegetation native to the southern united states. *Fuel* 229:151–66. doi:10.1016/j.fuel.2018.04.166.

Sheng, C., and J. Azevedo. 2002. Modeling biomass devolatilization using the chemical percolation devolatilization model for the main components. *Proc. Combust. Inst.* 29 (1):407–14. doi:10.1016/S1540-7489(02)80054-2.

Shotorban, B., B. L. Yashwanth, S. Mahalingam, and D. J. Haring. 2018. An investigation of pyrolysis and ignition of moist leaf-like fuel subject to convective heating. *Combust. Flame* 190:25–35. doi:10.1016/j.combustflame.2017.11.008.

Snegirev, A., E. Kuznetsov, and E. Markus. 2017. Coupled analytical approach to predict piloted flaming ignition of non-charring polymers. *Fire Saf. J.* 93:74–83. doi:10.1016/j.firesaf.2017.08.006.

Syrodoy, S. V., G. V. Kuznetsov, N. Y. Gutareva, K. A. Bugaeva, and R. I. Taburchinov. 2018. The conditions and characteristics of wood particles ignition in the stream of the high temperature gases. *Combust. Sci. Technol.* 190 (4):663–86. doi:10.1080/00102202.2017.1404997.

Tihay, V., P.-A. Santoni, A. Simeoni, J.-P. Garo, and J.-P. Vantelon. 2009. Skeletal and global mechanisms for the combustion of gases released by crushed forest fuels. *Combust. Flame* 156 (8):1565–75. doi:10.1016/j.combustflame.2009.05.004.

Turns, S. R. (2000), 'An introduction to combustion', McGraw-hill.

Weise, D. R., E. Koo, X. Zhou, S. Mahalingam, F. Morandini, and J.-H. Balbi. 2016. Fire spread in chaparral–a comparison of laboratory data and model predictions in burning live fuels. *Int. J. Wildland Fire* 25 (9):980–94. doi:10.1071/WF15177.

Weise, D. R., X. Zhou, L. Sun, and S. Mahalingam. 2005. 'Fire spread in chaparral—'go or no-go?". *Int. J. Wildland Fire* 14 (1):99–106. doi:10.1071/WF04049.

Yashwanth, B., B. Shotorban, S. Mahalingam, C. Lautenberger, and D. Weise. 2016. A numerical investigation of the influence of radiation and moisture content on pyrolysis and ignition of a leaf-like fuel element. *Combust. Flame* 163:301–16. doi:10.1016/j.combustflame.2015.10.006.

Yashwanth, B. L., J. Gallacher, B. Shotorban, S. Mahalingam, T. H. Fletcher, and D. R. Weise (2015), Experimental and numerical investigation of the effect of heating modes and moisture content on pyrolysis and ignition of live fuels, *in* '9th US National Meeting Organized by the Central States Section of the Combustion Institute', Cincinnati, OH.

Appendix A. Mathematical Formulation of Pyrolyzing Fuel

Three-dimensional condensed-phase equations of mass, species and energy conservation are, respectively (Shotorban et al. 2018).

$$\frac{\partial \bar{\rho}}{\partial t} = -\dot{\omega}'''_{fg}, \tag{A.1}$$

$$\frac{\partial (\bar{\rho} Y_i)}{\partial t} = \dot{\omega}'''_{fi} - \dot{\omega}'''_{di}, \tag{A.2}$$

$$\frac{\partial\left(\bar{\rho}\tilde{h}\right)}{\partial t} = - \quad \cdot \dot{\mathbf{q}}'' - \dot{Q}'''_{s-g}, + \sum_k \dot{Q}'''_{s,k} - \frac{\partial \dot{q}''_r}{\partial z} + \sum_i \left(\dot{\omega}'''_{fi} - \dot{\omega}'''_{di}\right) h_i. \tag{A.3}$$

where $\bar{\rho}$ is the condensed phase overall density, Y_i is condensed species mass fraction, $\dot{\omega}'''_{fg}$, $\dot{\omega}'''_{fi}$ and $\dot{\omega}'''_{di}$ are the volumetric reaction rates of total gas formation, species i formation and species i destruction, respectively, $\dot{Q}'''_{s-g}$ is the volumetric rate of heat transfer from the condensed phase to the gas phase, which is correlated with the volumetric rate of heat release due to homogeneous gaseous reactions, $\dot{Q}'''_{s,k}$ is the volumetric rate of heat release (or absorption) due to condensed phase reactions, $\dot{\mathbf{q}}'' = -\bar{k} \quad T$ is the conduction heat flux vector, $\dot{q}''_r$ is the in-depth radiative heat flux, and h_i is the enthalpy of species i, and $\tilde{h} = \sum_i Y_i h_i$ is the mass-based averaged enthalpy. Eqs (A.1-A.3) look identical to the conservation equations given in the technical manual of Gpyro (Lautenberger 2014) for a three dimensional domain with no volume change. However, the overbar that indicates the volumetric average is defined differently here, as illustrated by Shotorban et al. (2018). The new definition removes the mathematical constraint needed to be imposed on the densities of the condensed phase to satisfy the no volume change condition. For the gas phase within the solid fuel, the following three-dimensional equations of mass and species conservation are solved

$$\frac{\partial\left(\rho_g \bar{\psi}\right)}{\partial t} + \quad \cdot \dot{\mathbf{m}}'' = \dot{\omega}''_{fg}, \tag{A.4}$$

$$\frac{\partial\left(\rho_g \bar{\psi} Y_j\right)}{\partial t} + \quad \cdot \dot{\mathbf{m}}'' Y_j = - \quad \cdot \dot{\mathbf{j}}''_j + \dot{\omega}'''_{fj} - \dot{\omega}'''_{dj}, \tag{A.5}$$

where ρ_g and $\bar{\psi}$ are the gas phase overall density and porosity, respectively, $\dot{\mathbf{m}}'' = -\left(\overline{K}/\nu\right)\left(\quad P - \rho_g \boldsymbol{g}\right)$ and $\boldsymbol{j}''_j = -\overline{\psi}\rho_g \boldsymbol{D} \quad \boldsymbol{Y_j}$ are the total convective flux and diffusive flux of species j, respectively, Y_j is the mass fraction of the gas species j, and ν, K, and D are viscosity, permeability and diffusivity, respectively. Here, g indicates the gravitational acceleration vector. Under the assumption that the gas phase is in thermal equilibrium with the condensed phase, the local gas- and condensed-phase temperatures are identical.

The utilized boundary and initial conditions (Yashwanth et al. 2016) are illustrated here. The boundary condition for the energy is:

$$\bar{k} \quad T_s.\mathbf{n} = \bar{\varepsilon}\dot{q}''_{\text{incident}} - \bar{\varepsilon}\sigma {T_s}^4 - h_c(T_s - T_\infty) \tag{A.6}$$

where $\mathbf{n}$ is the unit vector normal to the solid fuel surface, $\bar{k}$ and $\bar{\varepsilon}$ are the volume-averaged heat conductivity and emissivity of the condensed phase, respectively, σ is the Stefan-Boltzman constant, and T_s is the solid fuel surface temperature. Here, $\dot{q}''_{\text{incident}}$, h_c, and T_∞ are incident radiant heat flux on the solid fuel surface, convective heat transfer coefficient and temperature in the gas phase (FDS) domain right next to the solid fuel. For the gas species conservation equation (A.5), the boundary condition given below is used:

$$\dot{\mathbf{m}}''_{j,s} \cdot \mathbf{n} - Y_{j,s}\, \dot{\mathbf{m}}''_s \cdot \mathbf{n} = h_m(Y_{j,s} - Y_{j,\infty}), \tag{A.7}$$

where $\dot{\mathbf{m}}''_{j,s}$ is the total mass flux (convective and diffusive) of the gas species j and $\dot{\mathbf{m}}''_s$ is the gas total mass flux at the solid fuel surface. Here, $h_m = h_c/c_{p,g}$ is the mass transfer coefficient where where $c_{p,g}$ is the specific heat of the gas and $Y_{j,\infty}$ is the mass fraction of the gas species j in the gas phase domain right next to the solid fuel. Initially, the solid fuel is at the ambient temperature, i.e. 300 K, its composition is known and its pores are filled with atmospheric air.